scientific reports

Check for updates

OPEN

Human umbilical cord-derived mesenchymal stem cells improve thymus and spleen functions in D-galactose-induced aged mice

Jianwei Xu[1,2,11], Li Dong[3,11], Xiaofen Xie[2], Bill D. Geng[4], Junhou Lu[5], Yongxi Dong[3], Yang Hu[6], Can Liu[2,7], Yuanhu Mao[3], Guo Ge[8,9]✉ & Zhenkui Ren[10]✉

As aging progresses, the structures and functions of immune organs such as the thymus and spleen deteriorate, leading to impaired immune function and immune senescence. This study investigated the potential of umbilical cord mesenchymal stem cells (UC-MSCs) to mitigate D-galactose-induced immune senescence by enhancing the structural and functional integrity of aging immune organs and regulating the gut microbiota. The findings show that UC-MSCs treatment significantly delayed thymus and spleen atrophy and reduced the number of senescence-associated β-galactosidase (SA-β-gal) positive cells. At the molecular level, UC-MSCs treatment downregulated the expression of aging-related genes, including p16, p53, p21, and RB. It also boosted antioxidant enzyme activity, increasing the levels of catalase (CAT), superoxide dismutase (SOD), and glutathione peroxidase (GSH-Px), while decreasing serum malondialdehyde (MDA) levels by activating the Nrf2/HO-1 pathway. Additionally, UC-MSCs treatment restored the balance of the gut microbiota. These results demonstrate that UC-MSCs significantly improve the structural and functional integrity of immune organs and enhance the composition of the gut microbiome, offering a potential strategy for delaying immune senescence.

Keywords Human umbilical cord-derived mesenchymal stem cells, Aging, Thymus and spleen, Nrf2/HO-1, Gut microbiota

Aging is characterized by the progressive decline in cellular, tissue, and organ function, resulting in an increased susceptibility to disease and ultimately death[1]. A principal hallmark of aging is immunosenescence which is closely associated with thymus degeneration and impaired spleen function[2,3]. Consequently, rejuvenating these immune components may offer a promising therapeutic strategy for attenuating the aging process.

The gene expression dysfunction mechanisms downstream Nrf2/HO-1 pathway could be responsible for decreased antioxidant capacity during aging[4,5]. Qian et. al. found that *Lactobacillus Plantarum* LP-CQPC11 inhibited D-galactose-induced oxidative stress and aging in mice by upregulating the Nrf2/HO-1 pathway[6]. In addition, alterations in the composition, diversity, and functional characteristics of gut microbiota are believed to be intricately linked to the aging process[7]. A relevant study has demonstrated that administering probiotic fermented milk supplements to aged mice mitigated immune decline, enhanced antioxidant enzyme activities, and improved resistance to *Escherichia coli* infection[8]. Mesenchymal stromal cells are a type of pluripotent adult stem cells with the capacity to self-renew and differentiate into a variety of cell lineages[9,10]. Wang et al. demonstrated in their study that bone marrow mesenchymal stem cells could mitigate age-related changes in the spleen and thymus by regulating oxidative stress and modulating P21/PCNA expression[11]. In a rat model of thymus aging, Jung et al. validated that adipose-derived mesenchymal stem cells induced regenerative effects

[1]Center for Tissue Engineering and Stem Cell Research, Guizhou Medical University, Guiyang, China. [2]Department of Pharmacology, School of Basic Medicine, Guizhou Medical University, Guiyang, China. [3]School of Pharmacy, Guizhou Medical University, Guiyang, China. [4]School of Natural Science, University of Texas at Austin, Austin, USA. [5]Translational Medicine Research Center, Guizhou Medical University, Guiyang, China. [6]Children's Medical Center, Affiliated Hospital of Guizhou Medical University, Guiyang, China. [7]Guizhong Biotechnology Co., Ltd., Guiyang, China. [8]Key Laboratory of Medical Biology, Guizhou Medical University, Ankang Avenue, Gui'an New District, China. [9]Department of Human Anatomy, School of Basic Medicine, Guizhou Medical University, Guiyang, China. [10]Clinical Laboratory, Second People's Hospital of Guizhou Province, 206 South Section of Xintian Avenue, Guiyang City, China. [11]Jianwei Xu and Li Dong have contributed equally to this work. ✉email: guoge113@163.com; 2639092792@qq.com

characterized by increased thymus volume and weight, as well as enhanced proliferation of the thymic epithelial cell line[12]. As a result, mesenchymal stem cells showed significant potential to improve both structural and functional aspects of the thymus and spleen. Umbilical cord mesenchymal stem cells (UC-MSCs), derived from neonatal cord tissue, possess enhanced self-renewal capacity, robust proliferation potential, and multi-lineage differentiation ability[13,14]. However, there has been limited research conducted on the use of UC-MSCs to counteract aging in these organs.

The key characteristics of aging include genomic instability, telomere shortening, epigenetic changes, loss of protein balance, disrupted nutrient sensing, mitochondrial dysfunction, cellular senescence, stem cell depletion, and altered intercellular communication. This study focuses on aging in immune organs—thymus and spleen, umbilical cord-derived mesenchymal stem cells (UC-MSCs), and the gut microbiota. It aims to evaluate whether UC-MSCs could alleviate thymic and splenic aging in D-galactose-induced senescent mice by modulating gut microbiota balance and reducing oxidative stress. Additionally, the study explored the potential link between these effects and the Nrf2/HO-1 signaling pathway, offering a prospective strategy for delaying immunosenescence.

Materials and methods

Mice

Thirty Kunming mice (eight weeks old, 20 ± 2 g body weight) were purchased from the Guizhou Medical University Laboratory Animal Center (license approval number: SCXK [Jing] 2019–0010, Beijing, China). The mice were housed in the standard animal laboratory of Guizhou Medical University's Tissue Engineering and Stem Cell Experiment Center. The laboratory conditions were maintained at a temperature of 20–25 °C and a humidity level of 30–40%, with alternating light and dark cycles of 12 h. The mice had access to water ad libitum and were fed a standard chow pellet diet. Animal Ethics Committee of Guizhou Medical University reviewed and approved the experimental procedures (NO: 2001976, Guizhou, China). Mice were administered an intraperitoneal injection of pentobarbital sodium at a dose of 100 mg/kg body weight. The mice were housed in a clean, quiet environment and monitored for any signs of distress or pain. Once fully anesthetized and unresponsive to stimuli, they were removed from their cages and euthanized by cervical dislocation. All procedures were conducted in accordance with the Institutional Animal Care and Use Committee guidelines for animal euthanasia. Experimental protocols involving animals adhered to the National Institutes of Health Guide for the Care and Use of Laboratory Animals and were approved by the Human Ethics Committee of Guizhou Medical University (Approval Number: 2022–018). In addition, all studies and subsequent experiments complied with ARRIVE guidelines and other relevant regulations.

UC-MSCs isolation and culture

The newborn's human umbilical cord was obtained from the Department of Obstetrics and Gynecology at the Affiliated Hospital of Guizhou Medical University, with the informed consent of the mothers and approved by the Human Ethics Committee of the hospital. To prepare the umbilical cords from healthy newborns for stem cell extraction, the cords were washed with sterilized physiological saline solution to remove blood clots, then soaked in 75% ethanol for 30 s, and rinsed with sterilized physiological saline three times to ensure any residual ethanol was removed. Subsequently, the peeling off the umbilical cord's arteries and veins were removed from the umbilical cord, and discarded, and then separating the Wharton's Jelly surrounding the blood vessel was carefully separated. The Wharton's Jelly was then placed into a small sterilized container using aseptic forceps, and small tissue blocks of approximately 1 mm^3 were prepared with sterilized eye scissors. The Wharton's jelly tissue blocks were placed in the culture flask with L-DMEM supplemented and 10% fetal bovine serum (Gibco, USA). The cultures were maintained at 37 °C with 5% CO_2 (ThermoForma, USA), the medium was changed every three days, and the cells were sub-cultured upon reaching 80% confluence. Third passage cells were collected and subjected to flow cytometry (BD, USA) analysis to identify specific cell surface molecular markers CD105, CD45, CD90, and CD34.

Establishment of D-galactose-induced aging model and UC-MSCs transplantation

After acclimating to the environment for a week, 30 mice were randomly assigned to three groups with an equal distribution of sexes: an aging model group (D-gal), an aging model group with UC-MSCs treatment (UC-MSCs), and a control group (Control). The D-gal and UC-MSCs groups received a daily subcutaneous injection of D-gal dissolved in 0.9% normal saline at a dosage of 500 mg/kg/day for eight consecutive weeks, while the Control group received an equal volume of normal saline[15]. In the UC-MSCs groups, the mice treated with D-gal also received a single intraperitoneal injection of UC-MSCs at a concentration of 2×10^6 cells/300 μL per mouse; the Control and D-gal groups received an equal volume of normal saline instead[16,17]. UC-MSCs-treated mice were sacrificed four weeks after UC-MSCs administration. Fresh feces were quick- frozen in liquid nitrogen and stored at − 80 °C for 16S rDNA gene sequencing. Additionally, serum and tissue samples were collected for various analyses, including H&E, Masson, SA-β-Gal staining, blood routine and biochemical index determination, real-time PCR, and immunohistochemical analysis.

Photographing and determining viscera index

After the mice were sacrificed, the thymus and spleen tissues were excised and photographed to measure their size. In addition, the thymus and spleen were weighed to calculate the organ coefficient. This calculation is performed using the following formula: organ coefficient (mg / g) = organ weight (mg) / body weight (g).

Blood routine and serum biochemistry test

Blood samples were collected by removing the eyeballs upon completion of the experiment. The serum was obtained by centrifuging the samples at 3000 rpm for 10 min at 4 °C. Blood samples with anticoagulant were also collected without clotting. Blood white blood cell count (WBC), lymphocyte count (LYM#), and lymphocyte percentage (LYM%) levels were analyzed using an automated coagulation analyzer (STAGO-compact MAX, France), and serum immunoglobulin IgG and IgM levels were measured using an automatic biochemical analyzer (TBA-FX8, Japan). Following the manufacturer's instructions, the activities of malondialdehyde (MDA, Cat. #: A003-1), Glutathione peroxidase (GSH-Px, Cat. #: A005-1), superoxide dismutase (SOD, Cat. #: A001-3), and catalase (CAT, Cat. #: A007-1–1) in serum were determined using commercial kits (Nanjing Jiancheng Bioengineering Institute, Nanjing, China).

Immunohistochemistry and histological staining

The thymus and spleen tissues were fixed in 4% paraformaldehyde for 24 h. After fixation, the tissues were embedded in paraffin and cut into 4 mm thick sections. For immunohistochemistry analysis, the sample was dewaxed in dimethyl and rehydrated in alcohol. Subsequently, the antigen was retrieved in complete citrate buffer (pH 6.0) and incubated with 3% hydrogen peroxide at room temperature in the dark for 25 min. Then specific antibodies were incubated overnight at 4℃. The proteins were detected using 3,3'-diaminobenzidine staining, while the nucleus was stained with hematoxylin. Tissue HO-1 and Nrf2 expression were evaluated using a microscope (Olympus, Japan).

The pathologic architecture and degree of fibrosis were examined using H&E and Masson's trichrome, respectively. Section imaging was carried out using a digital pathological section scanner (Olympus, Japan) to observe pathological changes.

Senescence-associated β-galactosidase (SA-β-Gal) staining

After dissecting the mice, the thymus and spleen tissues were separated and immediately stored in a deep freezer at − 80 °C. Subsequently, 5 μm-thick frozen sections were prepared using a CryoStar NX50 freezing microtome (Thermo Scientific, USA). The percentage of aging cells was determined by using an SA-β-gal staining kit (Beyotime, Shanghai, China). The sections were first fixed with the kit fixing solution for 20 min, washed with PBS buffer, and then subjected to overnight incubation in an SA-Gal staining solution at 37 °C. After 48 h of incubation, the samples were washed with PBS, covered with coverslips, and imaged using a microscope (Olympus, Japan).

Cytokine assay

Following the instructions provided by the manufacturer, the ELISA kit was used to determine the levels of interleukin-2 (IL-2, Cat.# VAL604-96, R&D Systems), interleukin-6 (IL-6, Cat.# VAL602-96, R&D Systems), and tumor necrosis factor-α (TNF-α, Cat.# VAL609-96, R&D Systems) in the serum.

RNA extraction and real-time fluorescence quantitative PCR

The total RNA of the thymus and spleen was extracted using the ES Science Plus tissue RNA rapid extraction kit. The target gene-specific primers, including IL-2, IL-6, TNF-α, p53, p21, p16, RB, Keap1, HO-1, Nrf2, and GAPDH genes were designed and synthesized by Shanghai Thermo Fisher Technology Co., Ltd. (Shanghai). The total RNA was undergoing reverse transcription into cDNA following the instructions from the reverse transcription kit (RR047A-100, TtaKaRa Japan). The cDNA was then amplified with Takara TB Green Premix Ex Taq (Takara, Japan) by using specific primers with a Bio-Rad CFX96 real-time PCR system (Bio-Rad, USA). The reaction conditions were set as follows: 95 °C for 30 s and followed by 40 cycles of 95 °C for 5 s and 60 °C for 30 s. GAPDH was used as an internal control. The $2-\Delta\Delta Ct$ values were used to assess mRNA expression levels. The primer sequences utilized for RT-qPCR are detailed in Table 1.

Gene	Forward primer (5' to 3')	Reverse primer (5' to 3')
RB	TCGATACGAGTACCAAGGTTGA	ACACGTCCGTTCTAATTTGCTG
p16	ACATCAAGACATCGTGCGATATT	CCAGCGGTACACAAAGACCA
p21	TGTCTTGCACTCTGGTGTCTG	ATCTGCGCTTGGAGTGATAGA
p53	TGGAAGGAAAATTTGTATCCCGA	GTGGATGGTGGTATACTCAGAG
IL-2	TCTGCGGCATGTTCTGGATTT	ATGTGTTGTCAGAGCCCTTTAG
IL-6	CTGCAAGAGACTTCCATCCAG	AGTGGTATAGACAGGTCTGTTGG
TNF-α	CCCTCACACTCAGATCATCTTCT	GCTACGACGTGGGCTACAG
Keap1	TGCCCCTGTGGTCAAAGTG	GGTTCGGTTACCGTCCTGC
HO-1	AAGCCGAGAATGCTGAGTTCA	GCCGTGTAGATGGTACAAGGA
Nrf2	GTGCTCCTATGCGTGAAT	TACCTCTCCTGCGTATATCT
GAPDH	AAGGTCATCCATGACAACTTTGGC	ACAGTCTTCTGGGTGGCAGTGAT

Table 1. Quantitative real-time PCR primer sequences.

Gut microbiota sequencing

Genomic DNA was extracted from mouse feces using DNeasy® PowerSoil® Pro Kit (Illumina, USA). The quantity and quality of genomic DNA were determined by NanoDrop2000 spectrophotometer and agarose gel electrophoresis, respectively. PCR primers were designed based on the conserved regions of the sequence, and specific barcode sequences were incorporated corresponding to the individual samples. PCR amplification of the 16 S V3-V4 region was followed by fluorescence quantification of the recovered PCR products. Based on the fluorescence quantification results, the samples were combined in corresponding proportions that were required for the sequencing volume. The sequencing library was constructed using NEB's NEXTFLEX Rapid DNA-Seq Kit, and subsequent high-throughput sequencing was carried out. The Miseq PE300/ NovaSeq PE300 platform was used to conduct all procedures, sequence analysis, and DNA extraction.

Statistical analysis

All experimental data were presented as mean ± SD. Statistical analyses were conducted using SPSS 26.0 Comparison among the different groups was subjected to statistical analysis using either a t-test or one-way analysis of variance, $p < 0.05$ was considered statistically significant.

Results

Identification and isolation of UC-MSCs

Human umbilical cord tissue blocks were seeded in 10 cm culture dishes based on the characteristics of adhesive growth of UC-MSCs. Within three days, a few elongated spindle-shaped cells were observed to emerge climb out, and adhere to the bottom of the dish's base. Upon continuous culture for 5–6 days, these cells exhibited rapid growth and spread throughout the surrounding area, and long spindle cells reached 80% coverage (Fig. 1a). After three passages, the cells appeared uniform and maintained their elongated spindle shape. After three consecutive subcultures, no discernible change in cell morphology was observed, indicating a high purification of UC-MSCs (Fig. 1b). Concurrently, UC-MSCs biomarkers were identified using flow cytometry. The analysis revealed 95.20% of the cells were positive for CD105 and 99.00% were positive for CD90, while only 0.051% were negative for CD45 and 0.036% were negative for CD34, confirming that the isolated cells were indeed UC-MSCs (Fig. 1c–f).

UC-MSCs improve thymus and spleen morphology and organ index

To investigate the impact of UC-MSCs on immune organs, we initially examined the effects of UC-MSCs on thymus and spleen morphology. Following UC-MSCs treatment, noticeable morphological alterations were observed in D-galactose-induced aging mice regarding their thymus and spleen. Visual inspection revealed a significant decrease in the volume of the thymus and spleen after D-galactose treatment, leading to a marked reduction in both the thymus and spleen indexes ($P < 0.01$). However, the administration of UC-MSCs reversed this effect substantially ($P < 0.01$, Fig. 2a, b).

Effects of UC-MSCs on blood routine and humoral immunity

Next, the effects of UC-MSCs on blood routine and humoral immunity were also examined. The WBC, LYM#, and LYM% levels in the aging D-gal group's whole blood were significantly lower than those in the Control group ($p < 0.01$, Fig. 2c–e). After intraperitoneal injection of UC-MSCs, the WBC, LYM#, and LYM% levels in the UC-MSCs group were significantly restored compared to the D-gal group ($p < 0.05$). Additionally, serum IgG and IgM levels in the D-gal group were lower than those in the Control group ($P < 0.01$). However, administering UC-MSCs increased serum IgG and IgM levels in mice ($P < 0.01$, Fig. 2f–g). This indicates potential therapeutic benefits for age-related immune system decline through UC-MSCs therapy.

Effect of UC-MSCs on the microstructure and senescence of spleen and thymus

In addition to examining the morphology of the thymus and spleen, we further investigated the impact of UC-MSCs on the microstructural features and senescence process. As shown in (Fig. 3a,b), in the Control group, there was a clear boundary between the cortex and the medulla. The cortex exhibited densely packed and deeply pigmented thymocytes, while the medulla contained numerous lightly pigmented thymic epithelial cells, and the thymic parenchyma area was large and full. In the D-gal group, the thymus displayed significant atrophy and degeneration, with a blurred junction between cortex and medulla, resulting in a smaller thymus parenchyma area. Compared with the D-gal group, the UC-MSCs treatment group exhibited an increase in the thymus parenchyma region. Furthermore, the structure of the cortex and medulla improved with clear boundaries becoming evident.

Furthermore, in the Control group, the size of splenic nodules exhibited uniform size, with a clear distinction boundary between white pulp and red pulp. Conversely, in the D-gal group, the spleen tissue displayed a relatively reduced proportion of white pulp, accompanied by an indistinct boundary between white pulp and splenic nodules. However, after UC-MSCs treatment, the size of splenic nodules was inconsistent, while the white pulp area showed an increase.

Additionally, Masson's trichrome staining showed a significant increase in collagen deposition within the thymus and spleen tissues of the D-gal group compared with the Control group. In contrast, in the UC-MSCs treatment group, there was a marked reduction in collagen deposition.

SA-β-Gal is a specific marker for cellular senescence. The results of SA-β-gal staining showed a significant increase in the percentage of SA-β-gal positive cells in the thymus and spleen tissues compared with the Control group ($P < 0.01$, Fig. 3a–d). In addition, UC-MSCs treatment effectively reduced the percentage of SA-β-gal positive cells in the thymus and spleen ($P < 0.01$). These results suggest that UC-MSCs treatment effectively alleviated D-galactose-induced aging in mice.

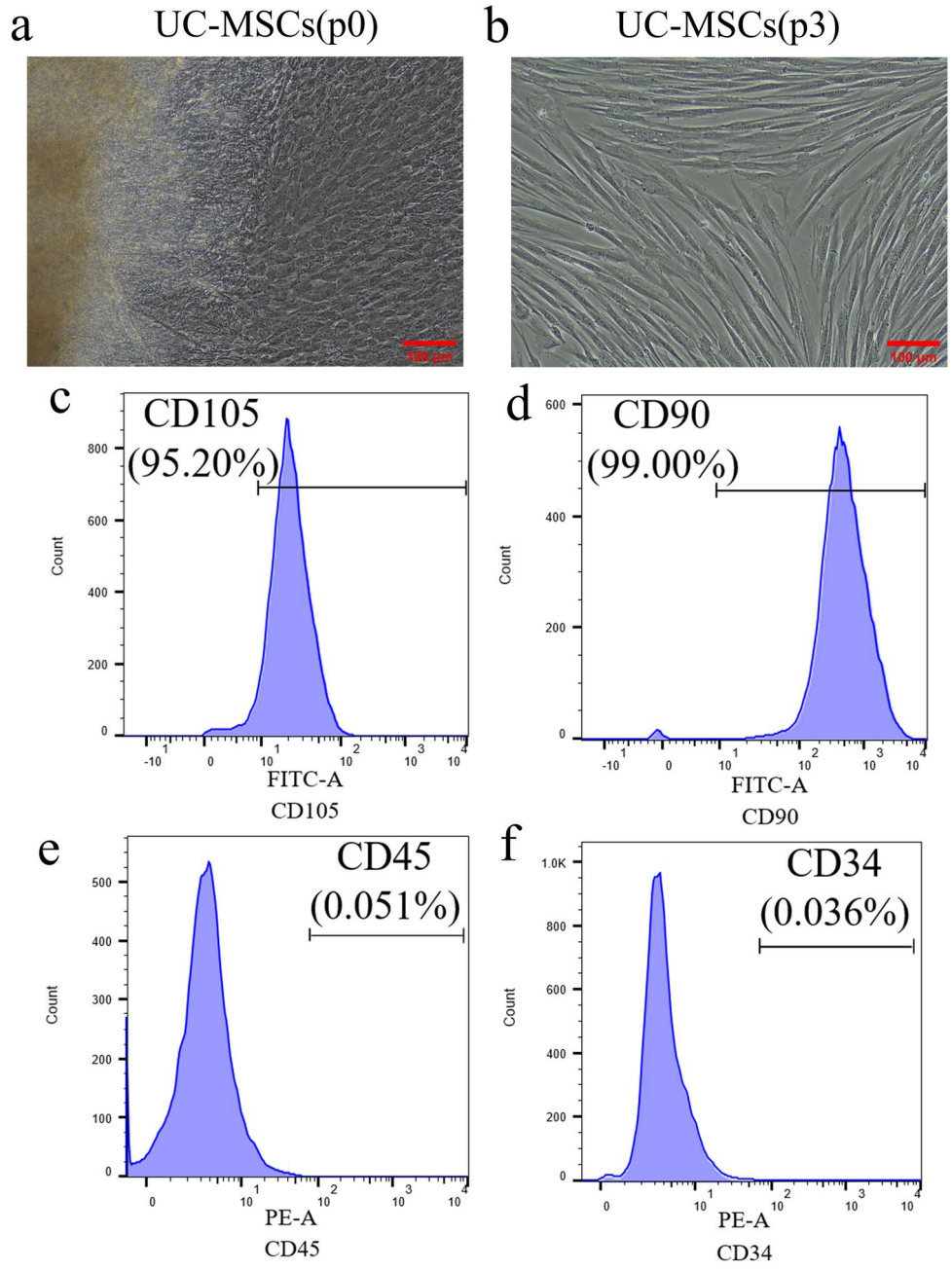

Fig. 1. Identification of human UC-MSCs. (**a**) Primary cultured UC-MSCs. Scale bar = 100 μm (**b**) Morphological feature of UC-MSCs at the third passage. Scale bar = 100 μm. The specific surface markers of cells were detected using flow cytometry, showing positive expression for (**c**) CD105 and (**d**) CD90, and negative expression for markers (**e**) CD45 and (**f**) CD34.

Taken together, these findings indicate that UC-MSCs may have potential therapeutic benefits for age-related changes seen within these important immune organs, and may be beneficial for preventing or reversing age-related degeneration.

Effect of UC-MSCs on oxidative stress in aging mice

To determine whether UC-MSCs have an effect on oxidative stress in D-gal-induced aging mice, we analyzed the levels of the antioxidant enzymes SOD, CAT, and GSH-PX, as well as the indicator of oxidative stress MDA. As shown in (Fig. 4a–d), compared to the Control group, the D-gal group exhibited a significant increase in the serum MDA activity, while the activities of SOD, CAT and GSH-PX were decreased ($P < 0.01$). Compared with the D-gal group, the UC-MSCs treatment group displayed significantly elevated activities of these antioxidant enzymes ($P < 0.01$), along with a considerable reduction in MDA ($P < 0.01$). These results suggest that UC-MSCs

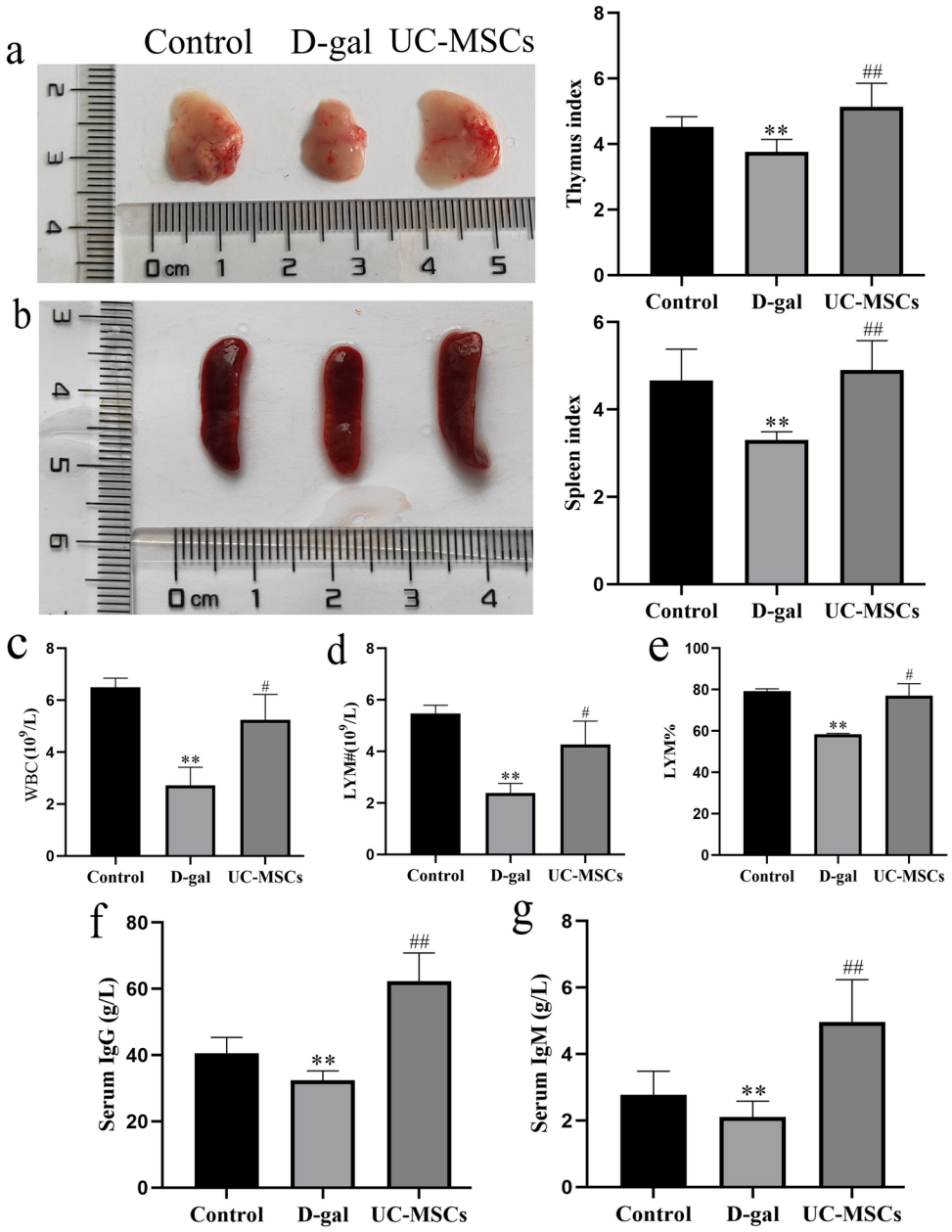

Fig. 2. Effects of UC-MSCs infusion on thymus and spleen tissue morphology, blood routine, and humoral immunity. The morphology dimensions and index of the thymus (**a**) and spleen (**b**). (**c**) White blood cell count (WBC). (**d**) Lymphocyte count (LYM#). (**e**) Lymphocyte percentage (LYM%). (**f**) Serum IgG and (**g**) serum IgM concentrations. Data are presented as means ± SD (n = 6). **p < 0.01* versus Control group; *#p < 0.05*, *##p < 0.01* versus D-gal group.

treatment has a positive impact on reducing oxidative stress in aging mice by enhancing their antioxidant defense system.

The effects of UC-MSCs on immune response and inflammation in aging mice

To evaluate the impact of UC-MSCs on immune response and inflammation, inflammatory cytokines TNF-α, IL-6, and IL-2 were assessed using ELISA. The results revealed that, compared to the D-gal group, the UC-MSCs group exhibited down-regulated TNF-α and IL-6 levels, while IL-2 levels were up-regulated (*P < 0.05*, *P < 0.01*, Fig. 5a–c). Moreover, real-time PCR analysis showed that the levels of IL-6 and TNF-α mRNA in the D-gal group were significantly higher than those in the Control group (*P < 0.01*, *P < 0.001*), and the level of IL-2 mRNA was lower than that in the Control group (*P < 0.05*, *P < 0.01*). However, UC-MSCs treatment significantly inhibited the elevation of IL-6 and TNF-α mRNA levels (*P < 0.01*, *P < 0.001*) and restored the decreased levels of IL-2 mRNA (*P < 0.01*, Fig. 5d–i). These changes at the gene expression level further corroborate the ELISA results

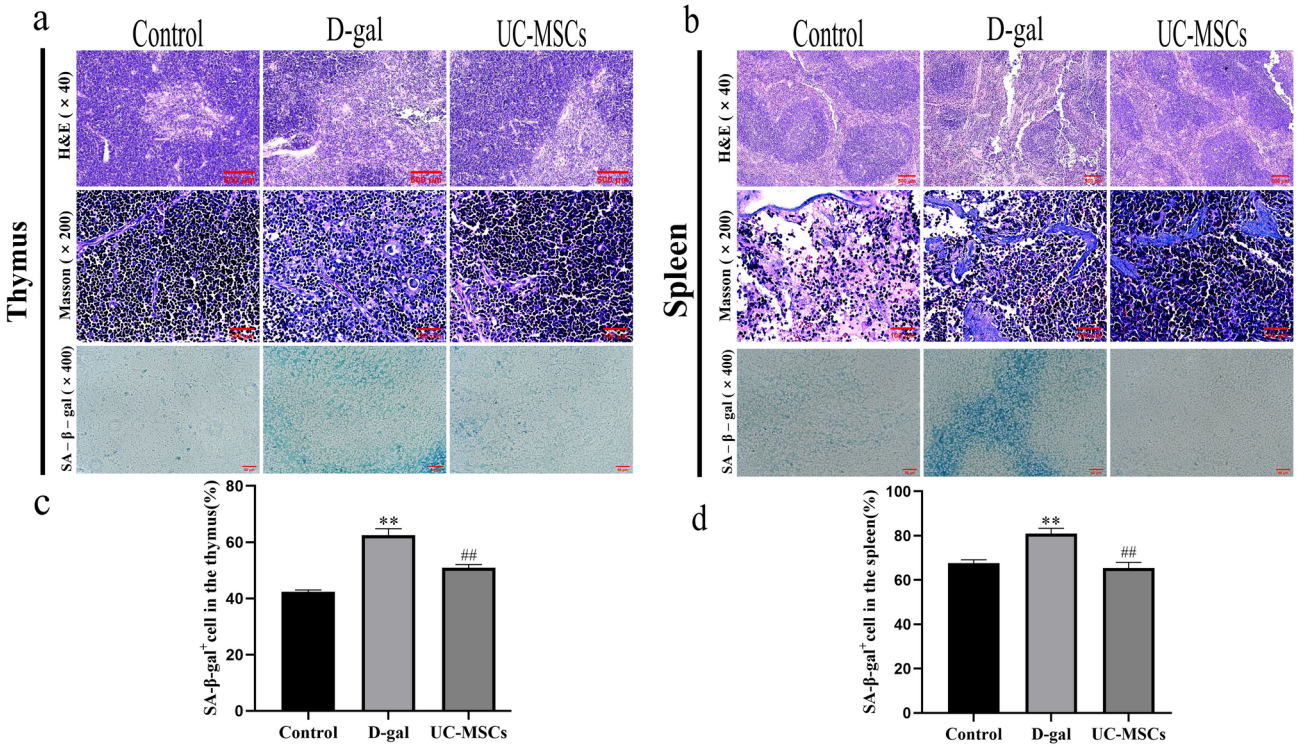

Fig. 3. H&E, Masson, and SA-β-gal staining in splenic and thymic tissue. (**a**) Histological staining showing collagen fiber and senescent cells in the thymus tissue. H&E: scale bar = 500 μm; Masson: scale bar = 100 μm; SA-B-gal: scale bar = 50 μm. (**b**) Histological staining showing collagen fiber and senescent cells in the spleen tissue. (**c**, **d**) Quantitative analysis of the effect of UC-MSCs on the ratio of senescent cells in the spleen and thymus. Data are presented as means ± SD (n = 3). **p < 0.01* versus Control group; *##p < 0.01* versus D-gal group.

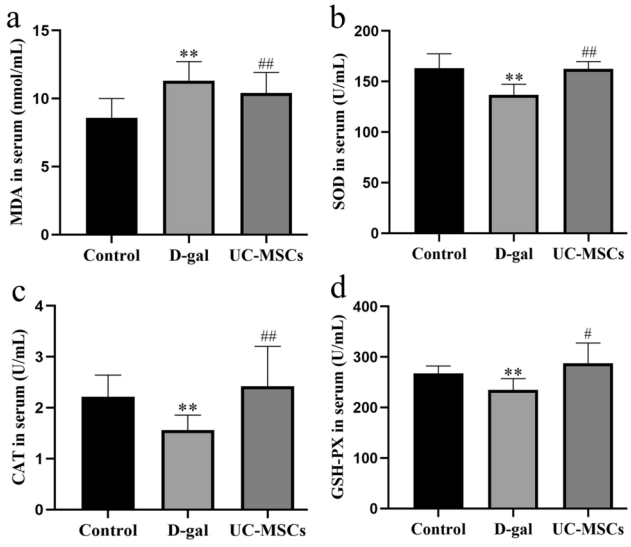

Fig. 4. Effect of UC-MSCs on oxidative stress in aging mice. (**a–d**) The activity levels of MDA, SOD, CAT, and GSH-PX in the serum. Data are presented as means ± SD (n = 6). **p < 0.01* versus Control group; *#p < 0.05*, *##p < 0.01* versus D-gal group.

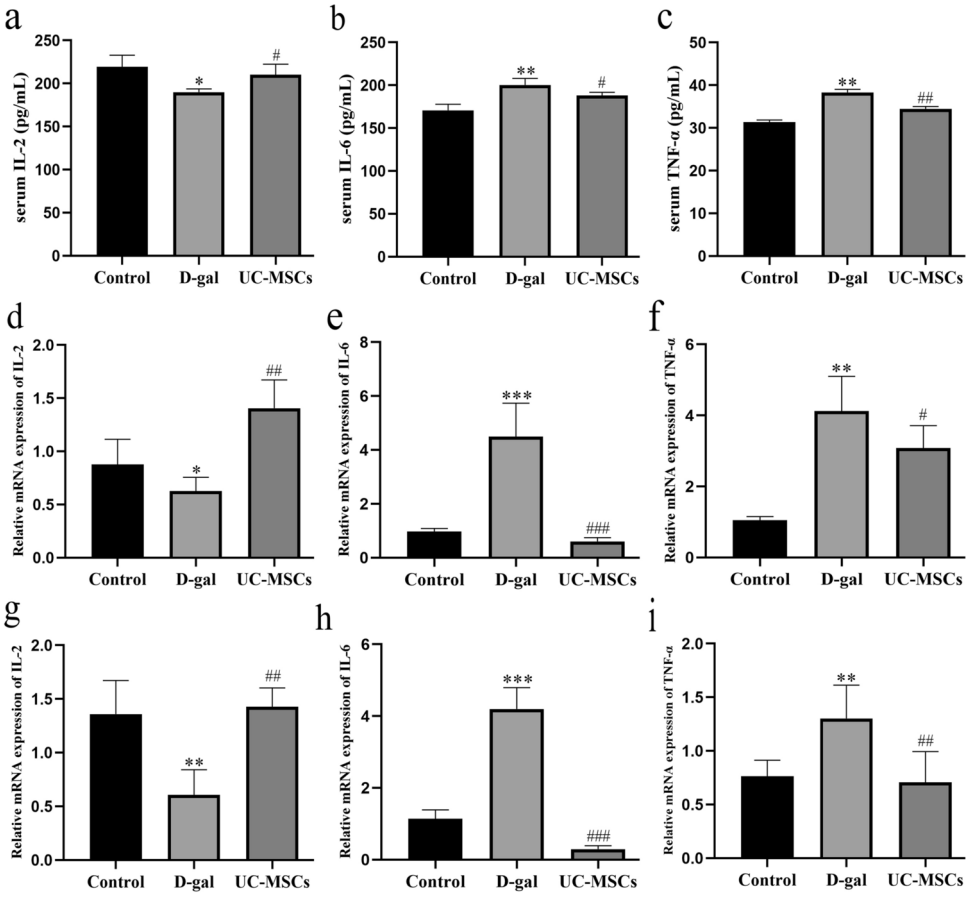

Fig. 5. Effect of UC-MSCs on cytokine in the serum, thymus, and spleen of aging mice. The levels of IL-2 (**a**), IL-6 (**b**), and TNF-α (**c**) in serum were determined using ELISA kits. The mRNA expression levels of IL-2 (**d**), IL-6 (**e**), and TNF-α (**f**) in the thymus were determined using RT-qPCR analysis. The mRNA expression levels of IL-2 (**g**), IL-6 (**h**), and TNF-α (**i**) in the spleen were determined using RT-qPCR analysis. Data are presented as means ± SD (n = 3). *$p < 0.05$, **$p < 0.01$, ***$p < 0.001$ versus Control group. #$p < 0.05$, ##$p < 0.01$, ###$p < 0.001$ versus D-gal group.

and underscore the immunomodulatory potential of UC-MSCs, as evidenced by their ability to decrease pro-inflammatory cytokines while increasing anti-inflammatory cytokines.

Effect of UC-MSCs on aging-related genes in aging mice

The p16-RB and p53-p21-RB pathways play crucial roles in signaling pathways for cellular senescence and cell cycle growth arrest. To further validate these findings, we performed real-time PCR to detect the expression of these senescence-related genes. The results showed a significant increase in the gene levels of RB, p16, p21, and p53 in the thymus and spleen tissues of the D-Gal group compared to those in the Control group ($P < 0.05$, $P < 0.01$). However, in mice treated with UC-MSCs, the RB, p16, p21, and p53 mRNA levels were significantly reversed compared to the D-gal group ($P < 0.05$, $P < 0.01$, Fig. 6a–h). These findings indicate that UC-MSCs have the potential to delay cellular senescence and further improve immunosenescence in the thymus and spleen by modulating p16-RB and p53 / p21 / RB pathways.

UC-MSCs alleviate immune aging by targeting the Nrf2 / HO-1 signaling pathway

The Nrf2 / HO-1 pathway is a crucial antioxidant regulatory pathway involved in the cellular senescence of macrophages and epithelial cells. We examined the effect of UC-MSCs on this pathway in the thymus and spleen tissues. The results showed that, compared to the Control group, the D-gal group exhibited decreased expression of Nrf2 and HO-1 mRNA, while the expression of Keap1 mRNA was significantly increased ($P < 0.05$, $P < 0.01$). In contrast, treatment with UC-MSCs led to increased Nrf2 and HO-1 mRNA expression, accompanied by a significant decrease in Keap1 mRNA expression ($P < 0.05$, $P < 0.01$, Fig. 7g, h). Immunohistochemical analysis showed that UC-MSCs treatment increased Nrf2 and HO-1 protein expression in the tissues ($P < 0.05$, $P < 0.01$, Fig. 7a–f). These results suggest that the Nrf2/HO-1 antioxidant pathway may play a role in mediating the effects of UC-MSCs in mitigating immunosenescence.

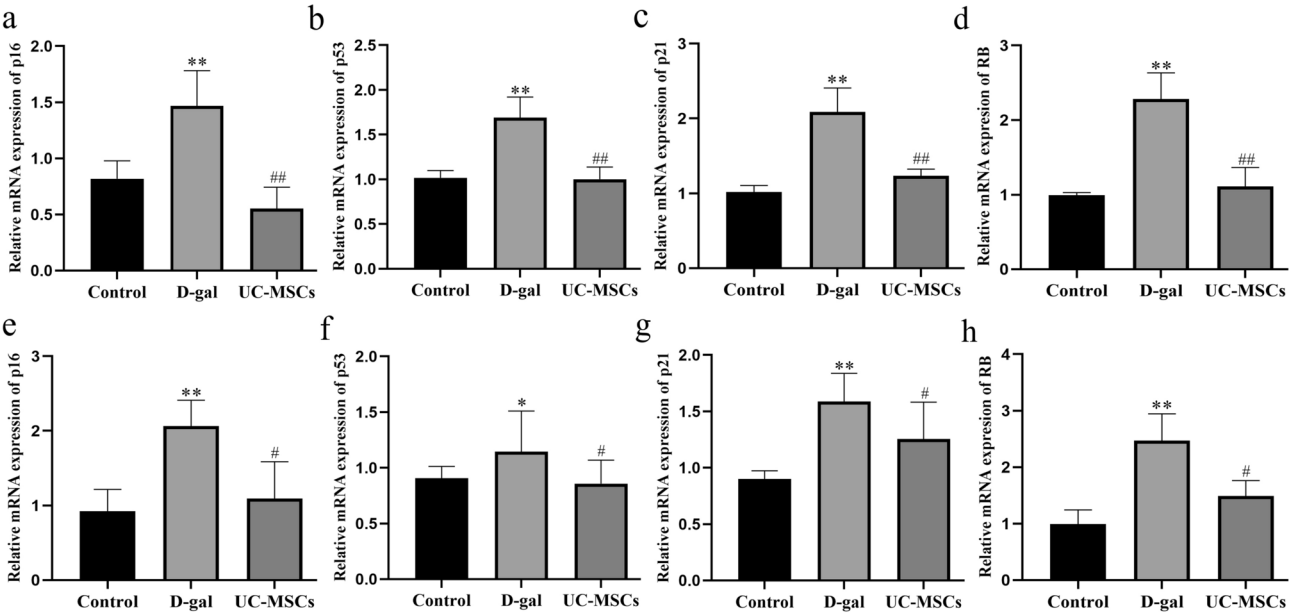

Fig. 6. UC-MSCs mitigate the aging of the thymus and spleen by regulating aging-related genes. (**a**-**d**) p16, p53, p21, and RB mRNA levels in the thymus. (**e**–**h**) p16, p53, p21, and RB mRNA levels in the spleen. Data are presented as means ± SD (n = 3). *$p < 0.05$, **$p < 0.01$ versus Control group. #$p < 0.05$, ##$p < 0.01$ versus D-gal group.

Improvement of α and β diversity in aging mice by UC-MSCs

To verify the comprehensiveness of microbial species in the sample, an abundance curve was used to evaluate the coverage of the 16S rDNA sequence. The Sobs curve (Fig. 8a) and the Shannon curve (Fig. 8b) approached a saturation plateau, signifying adequacy in the 16S rRNA gene sequence database generated using these sequences. This suggests that species richness in the sample is sufficient for subsequent analysis.

ANOSIM analysis indicated a greater difference among the three groups of mice compared to differences within the group (R = 0.6982, p = 0.01), and the difference was statistically significant (Fig. 8c).

Assessment of α diversity was carried out to investigate community distribution differences within the groups. Sobs, Chao, and Ace indexes, representing community richness, revealed an enriched gut microbiota in the D-gal group compared to the Control group ($P < 0.05$, $P < 0.01$), shown in (Fig. 8d–f). UC-MSCs treatment reduced the number of gut microbiota but without reaching statistical significance. Simpson and Shannon's indexes were used to determine the microbial community diversity and richness of microbial communities. A greater Simpson index and a smaller Shannon index indicate a higher species richness and diversity of a sample. Compared to the Control group, the D-gal group showed a reduction in the Shannon index ($P < 0.01$) and an increase in the Simpson index ($P < 0.01$). However, UC-MSCs treatment reversed this trend, and the differences were statistically significant ($P < 0.05$, $P < 0.01$, Fig. 8g, h). These results indicate that UC-MSCs treatment enhanced the richness and diversity of gut microbiota communities in the D-galactose-induced aging model mice.

Principal component analysis (PCA), principal coordinate analysis (PCoA), and non-metric multidimensional scaling (NMDS) based on Bray–Curtis analysis, were utilized to elucidate the difference and distance among samples by evaluating the OTU composition (97% similarity) from various samples. A smaller distance between the two samples suggests a more similar composition of the samples. The results of PCA (Fig. 8i), PCoA (Fig. 8j), and NMDS (Fig. 8k) revealed that, compared to the D-gal group, both the UC-MSCs treatment group and the Control group exhibited a more similar gut microbiota composition and closer distance.

The effect of UC-MSCs on community structure composition at phylum, genus, and family levels

Furthermore, we analyzed the microorganism differences in population and abundance among the three groups. Our results revealed that the top 10 microorganisms at the phylum, genus, and family levels displayed significant variations in the gut microbiota composition. At the phylum level, the dominant bacteria were *Firmicutes*, *Bacteroidetes*, and *Actinobacteria*. Compared to the Control group, D-gal administration significantly increased *Firmicutes* and *Actinobacteria* ($P < 0.05$) while decreasing *Bacteroidetes* ($P < 0.01$, Fig. 9a–d). However, UC-MSCs treatment reversed this change, resulting in reduced levels of *Firmicutes* and *Actinobacteria* ($P < 0.01$) and increased levels of *Bacteroidetes* ($P < 0.01$). At the genus level, the norank of *Muribaculaceae* bacterial community exhibited a significant decrease in the D-gal group compared to the Control group, while UC-MSCs treatment significantly increased this community ($P < 0.01$), Fig. 9e–h). Similarly, UC-MSCs administration restored the D-galactose-induced reduction of *Enterorhabdus* and *Corynebacterium* ($P < 0.01$). Moreover, at the family level, D-

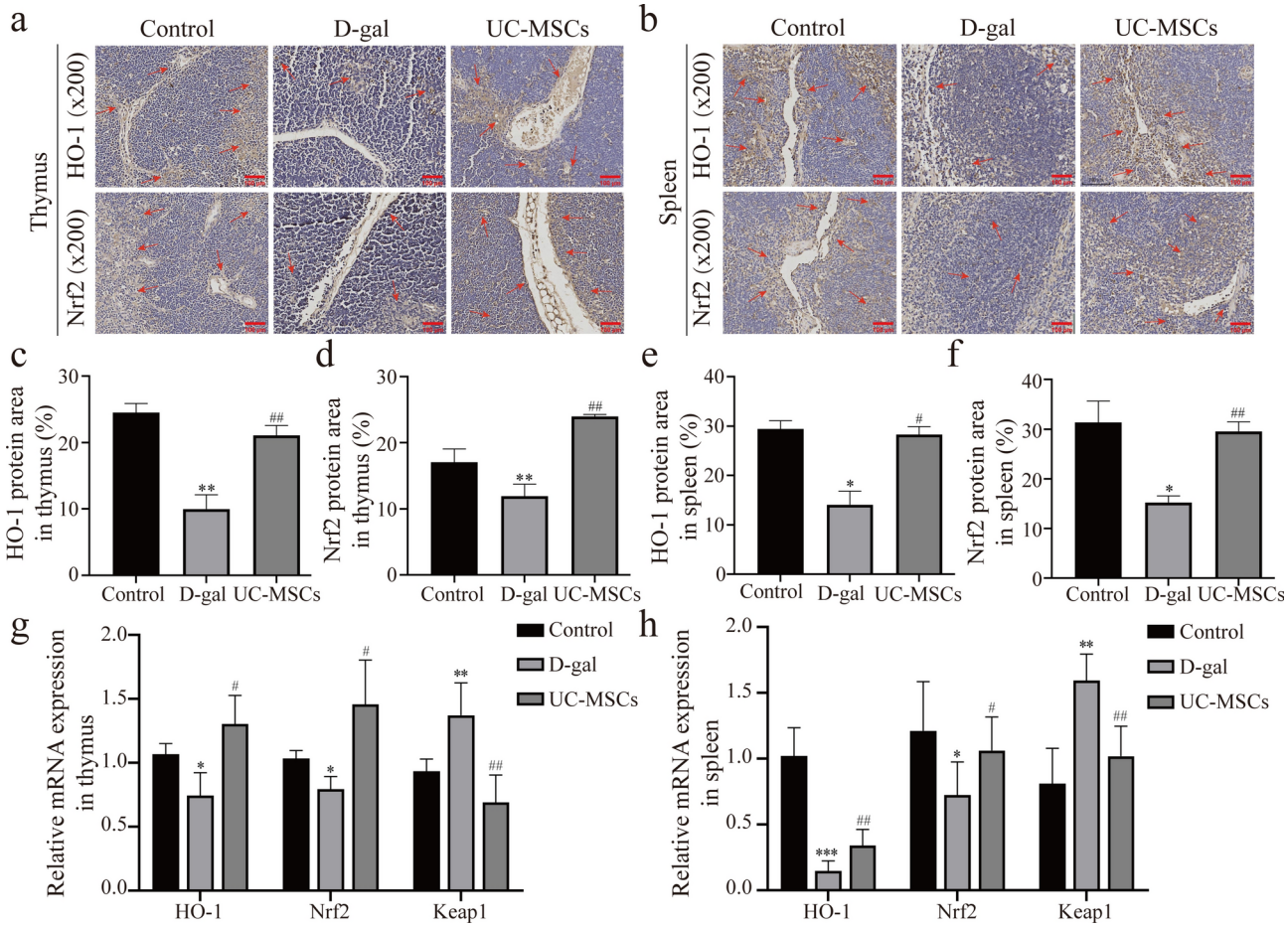

Fig. 7. UC-MSCs alleviate immune aging by regulating the Nrf2/HO-1 signaling pathway. (**a**-**f**) The impact of UC-MSCs on Nrf2 and HO-1 in the thymus(**a**, **c**, **d**) and spleen (**b**, **e**, **f**) tissues were assessed by immunohistochemical staining. The red arrows indicate the expression of Nrf2 and HO-1 proteins in the thymus and spleen tissues of mice in each group. Scale bar = 100 μm. HO-1, Nrf2, and Keap1 mRNA levels in the thymus (**g**) and spleen tissues (**h**) were measured by real-time PCR. Data were presented as means ± SD (n = 3). *$p < 0.05$, **$p < 0.01$ versus Control group. #$p < 0.05$, ##$p < 0.01$ versus D-gal group.

gal administration led to an increase in *Lactobacillaceae* and *Lachnospiraceae* and a decrease in *Muribaculaceae* compared to the Control group. However, UC-MSCs treatment reversed this change ($P < 0.5$, $P < 0.01$, Fig. 9i–l).

Analysis of differential species among groups

To further identify the specific bacterial groups related to the anti-aging of UC-MSCs, we employed LEfSe to compare the gut microbiota across different experimental groups. LEfSe analysis showed distinct differences in classification among the Control, the D-gal, and the UC-MSCs groups, identifying 6, 32, and 22 lineages respectively (Fig. 10a, b). The D-gal group exhibited five times more groups with significant differences compared to the Control group. In contrast, the number of groups in the UC-MSCs group decreased, positioning itself between the Control group and the D-gal group. This indicates that UC-MSCs have a restorative effect on the proliferation of specific flora in the feces of aging mice induced by D-gal. At the genus level, *Corynebacterium* predominated in the D-gal group, whereas norank_*Muribaculaceae* was the most prevalent in the UC-MSCs group. At the family level, *Prevotellaceae* emerged as the most dominant differential flora in the Control group, while *Enterococcaceae* exhibited prominence in the D-gal group, and *Muribaculaceae* was prevalent in the UC-MSCs group. In summary, our findings demonstrate that UC-MSCs can modulate the composition of gut microbiota in D-galactose-induced aging model mice.

Correlation analysis between gut microbiota composition and aging

Finally, we investigated the relationship between gut microbiota and aging using hierarchical clustering analysis and heat map visualization. The Spearman correlation coefficient was used to analyze the correlation between the top 30 dominant bacteria at the genus level and aging-related indicators in the thymus and spleen tissues, as well as in the serum. As shown in Fig. 11, *Corynebacterium* displayed a positive correlation with aging markers RB, p16, p21, and p53, while exhibiting a negative correlation with antioxidant enzymes SOD, CAT, and GSH-PX, as well as immunoglobulin IgG and IgM in the serum. It also showed a positive correlation with lipid peroxidation

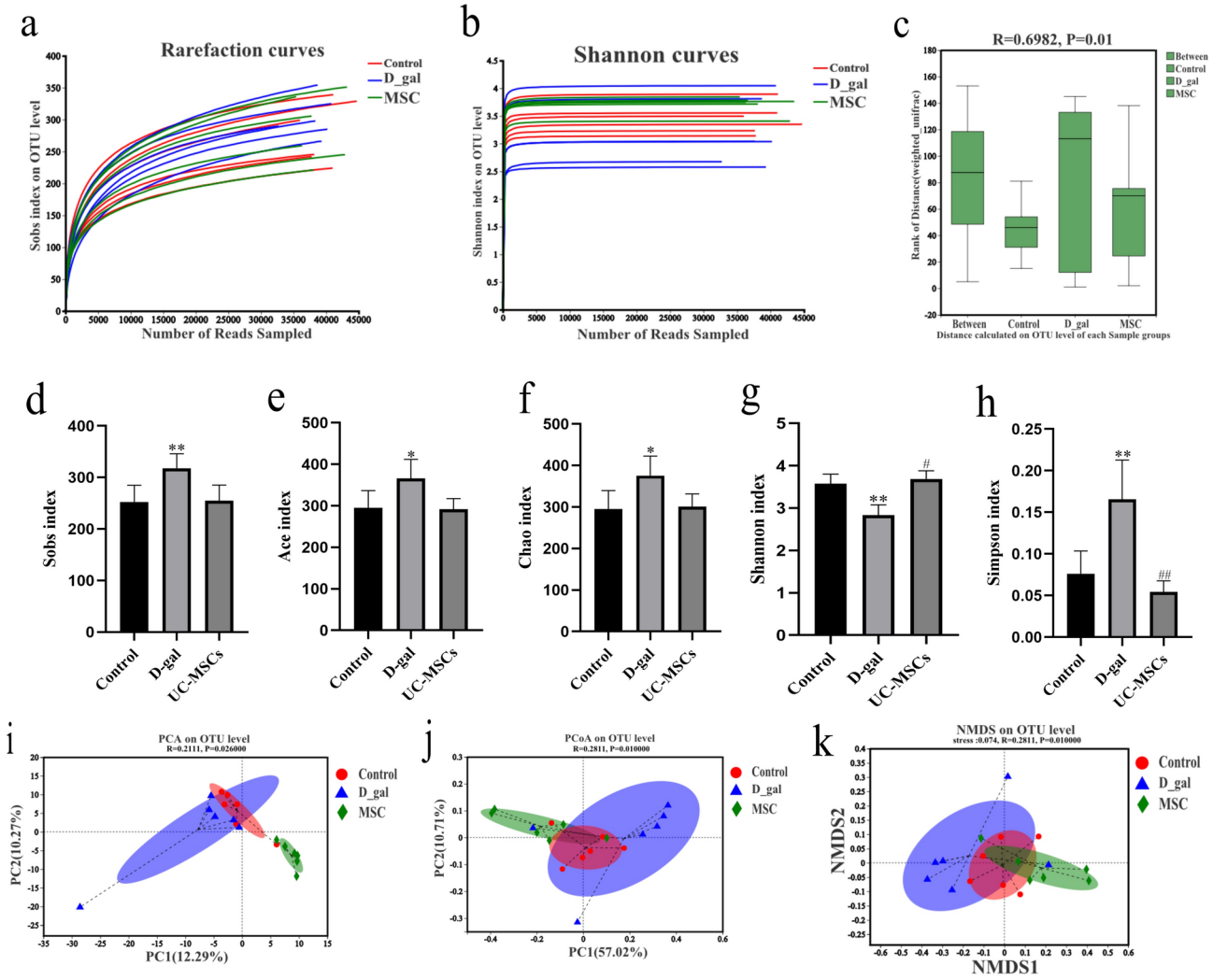

Fig. 8. UC-MSCs enhance α and β diversities in aging mice. (**a**) Rarefaction curve (Sobs). (**b**) Rarefaction curve (Shannon). (**c**) Unweighted UniFrac ANOSIM. (**d**) Sobs index. (**e**) Ace index. (**f**) Chao index. (**g**) Shannon index. (**h**) Simpson index. (**i**) Principal component analysis (PCA). (**j**) Principal coordinate analysis (PCoA). (**k**) Non-metric multi-dimensional scaling (NMDS).

product MDA, while being negatively correlated with thymus index and spleen index (*$p < 0.05$, **$p < 0.01$, and ***$p < 0.001$). In addition, *Corynebacterium* was negatively correlated with Nrf2 and HO-1 in the Nrf2 / HO-1 antioxidant pathway but positively correlated with Keap1 (**$p < 0.01$, and ***$p < 0.001$). Furthermore, our results demonstrated a positive correlation with cytokines TNF-α, and IL-6, and a negative correlation with IL-2 (*$p < 0.05$, **$p < 0.01$, and ***$p < 0.001$). *Alloprevotella*, on the other hand, was negatively correlated with RB, p16, p21, p53, TNF-α, IL-6, Keap1, and MDA, while presenting a positive correlation with Nrf2, HO-1, IL-2, thymus index, spleen index, SOD, CAT, GSH-PX, IgG, IgM (*$p < 0.05$, **$p < 0.01$, and ***$p < 0.001$). While *Odoribacter* exhibited a positive correlation with RB, p16, p21, p53, TNF-α, IL-6, Keap1, MDA, but a negative correlation with Nrf2, HO-1, IL-2, thymus index, spleen index SOD, CAT, GSH-PX, IgG, IgM (*p < 0.05, **p < 0.01, and ***p < 0.001). In summary, there appears to be a significant positive or negative correlation between aging-related indicators and various bacteria strains. These bacteria may be closely related to antioxidants and anti-aging processes.

Discussion

Immunosenescence refers to the deterioration of both the structure and function of the immune system, affecting various organs, cells, immune factors, and regulatory networks[18,19] As the site of T-cell development and maturation, the thymus gradually atrophies with age, leading to a significant decrease in thymocyte numbers[20]. This decline adversely impacts T-cell production and output, ultimately weakening immune system function[21]. Similarly, the spleen, a vital immune organ responsible for blood filtration and immune responses undergoes structural changes with aging[22]. The number of lymphocytes in the white pulp decreases, and the germinal center atrophies, impairing the ability of immune cells to proliferate and differentiate[23]. Additionally, the functions of macrophages and other cells within the red pulp may decline, reducing their ability to clear pathogens. The

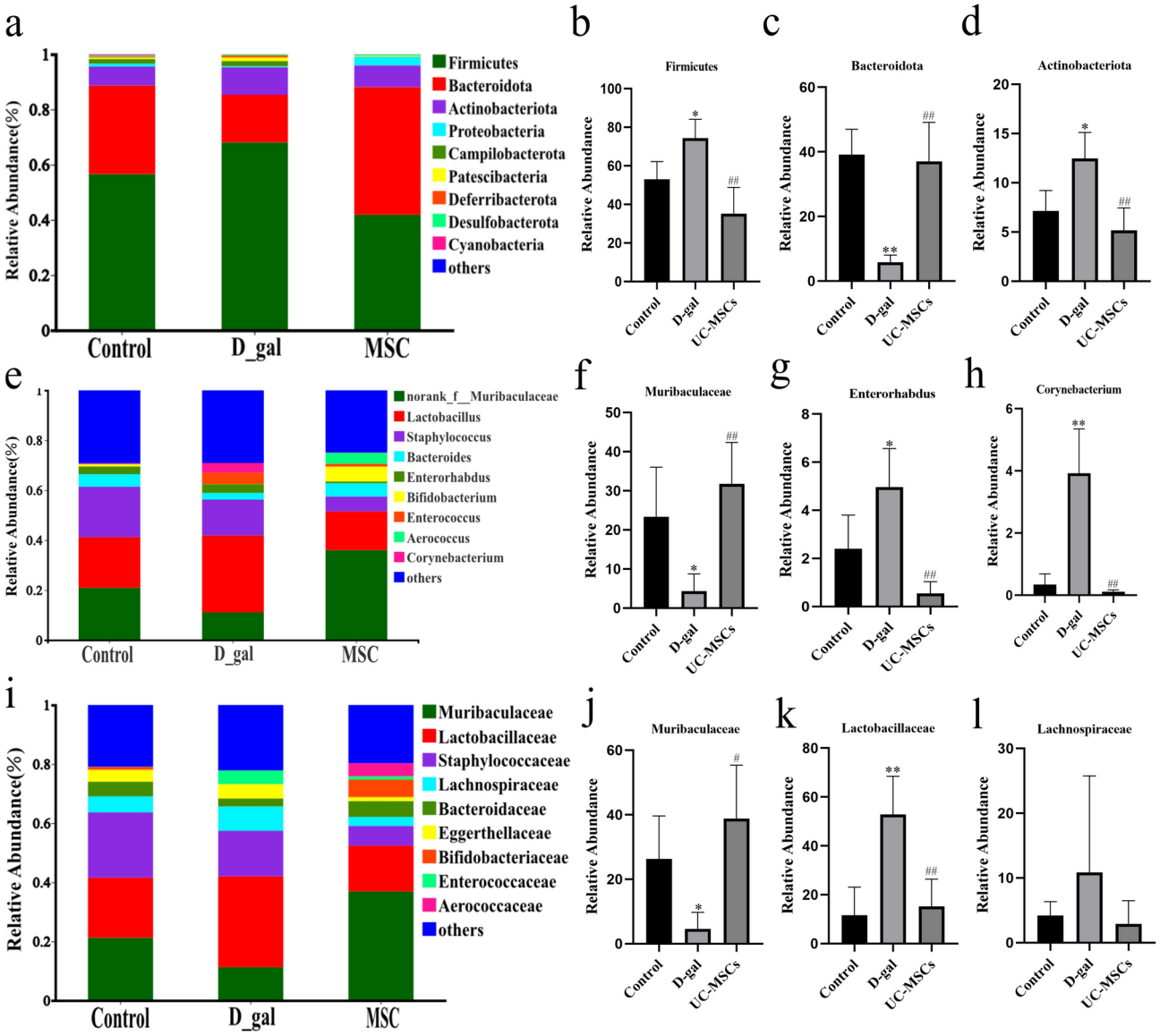

Fig. 9. Effects of UC-MSCs on community composition at phylum, genus, and family levels. (**a**) Relative abundance in phylum level (Top 10, phylum). (**b**-**d**) Relative abundance of *Firmicutes*, *Bacteroidetes*, and *Bacteroidetes*. (**e**) Relative abundance in genus level (Top 10, genus). (**f**–**h**) Relative abundance of *Muribaculaceae*, *Enterorhabdus*, and *Corynebacterium*. (**i**) Relative abundance at the family level (Top 10, family). (**j**-**l**) Relative abundance of *Muribaculaceae*, *Lactobacillaceae* and *Lachnospiraceae*. Data are presented as means ± SD (n = 6). $*p < 0.05$, $**p < 0.01$ versus Control group. $\#p < 0.05$, $\#\#p < 0.01$ versus D-gal group.

regulatory capacity of aging immune organs on the immune system diminishes, which can affect the immune system's self-tolerance mechanisms. Aging may also alter the secretion and regulation of cytokines, in which cytokines that promote immune responses may decrease, while cytokines that inhibit immune responses may increase, weakening the immune system's ability to effectively respond to pathogens[23,24].

The atrophy of immune organs, including the thymus and spleen, results in a reduction in the number, diversity, and surface receptor activity of T-lymphocytes[25,26]. While immunoglobulin levels, such as IgG and IgM, which reflect humoral immunity and immune response capacity, also decline with age[27,28]. Key cytokines such as TNF-α, IL-2, and IL-6, which are crucial in regulating immune function, are closely associated with aging[24,29]. Previous studies have demonstrated that bone marrow-derived mesenchymal stem cells attenuate D-galactose-induced senescence in $CD4^+$ T-cells by activating the Nrf2-mediated antioxidant defense system, thereby improving the functions of the thymus and spleen and inhibiting oxidative stress in aging rats[11,30]. Researchers have demonstrated that UC-MSCs can enhance immune responses by facilitating the maturation and activation of dendritic cells[31]. These cells are responsible for capturing and processing antigens, which they then present to T cells, thereby initiating adaptive immune responses[32]. Additionally, UC-MSCs play a role in regulating macrophage polarization, which further bolsters immune responses against pathogen invasion and tumor cells[33,34]. Here, our findings demonstrate that compared to the control group, the thymus, spleen, and

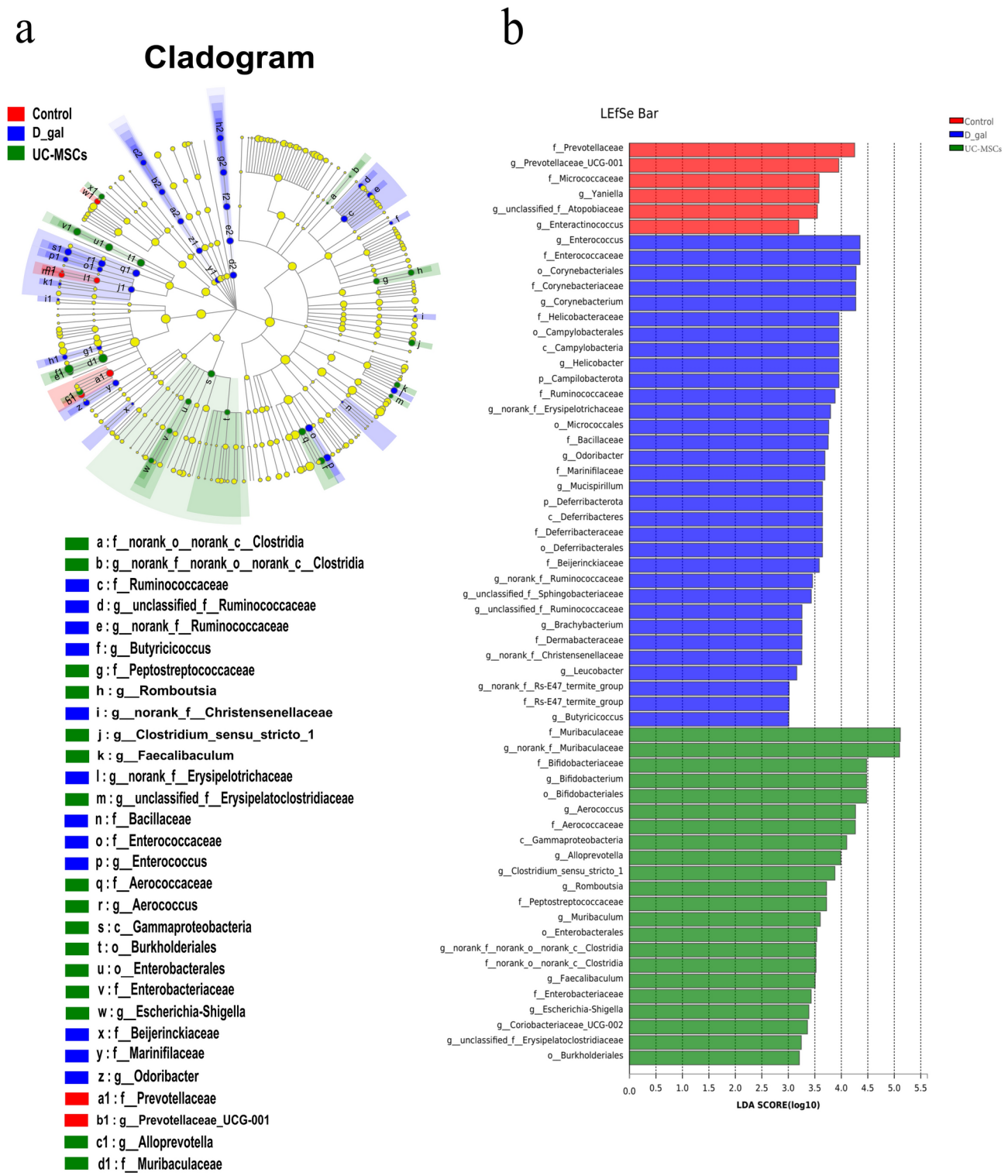

Fig. 10. Analysis of different species among the groups. (**a**) Linear discriminant analysis (LDA). (**b**) Statistical significance reflects $p < 0.05$ for Student's t-test, and LDA score threshold > 3 was listed, n = 6.

other immune organs in the D-galactose group exhibited significant atrophy, accompanied by a corresponding decrease in organ indices. In contrast, the UC-MSCs group showed increased organ indices, indicating that UC-MSCs can enhance the mass indices of the spleen and thymus in aging mice and inhibit the degeneration of immune organs. Additionally, aging mice showed significant decreases in WBC, LYM#, and LYM%, along with IgG, IgM, and IL-2 levels, while TNF-α and IL-6 increased. However, treatment with UC-MSCs improved these

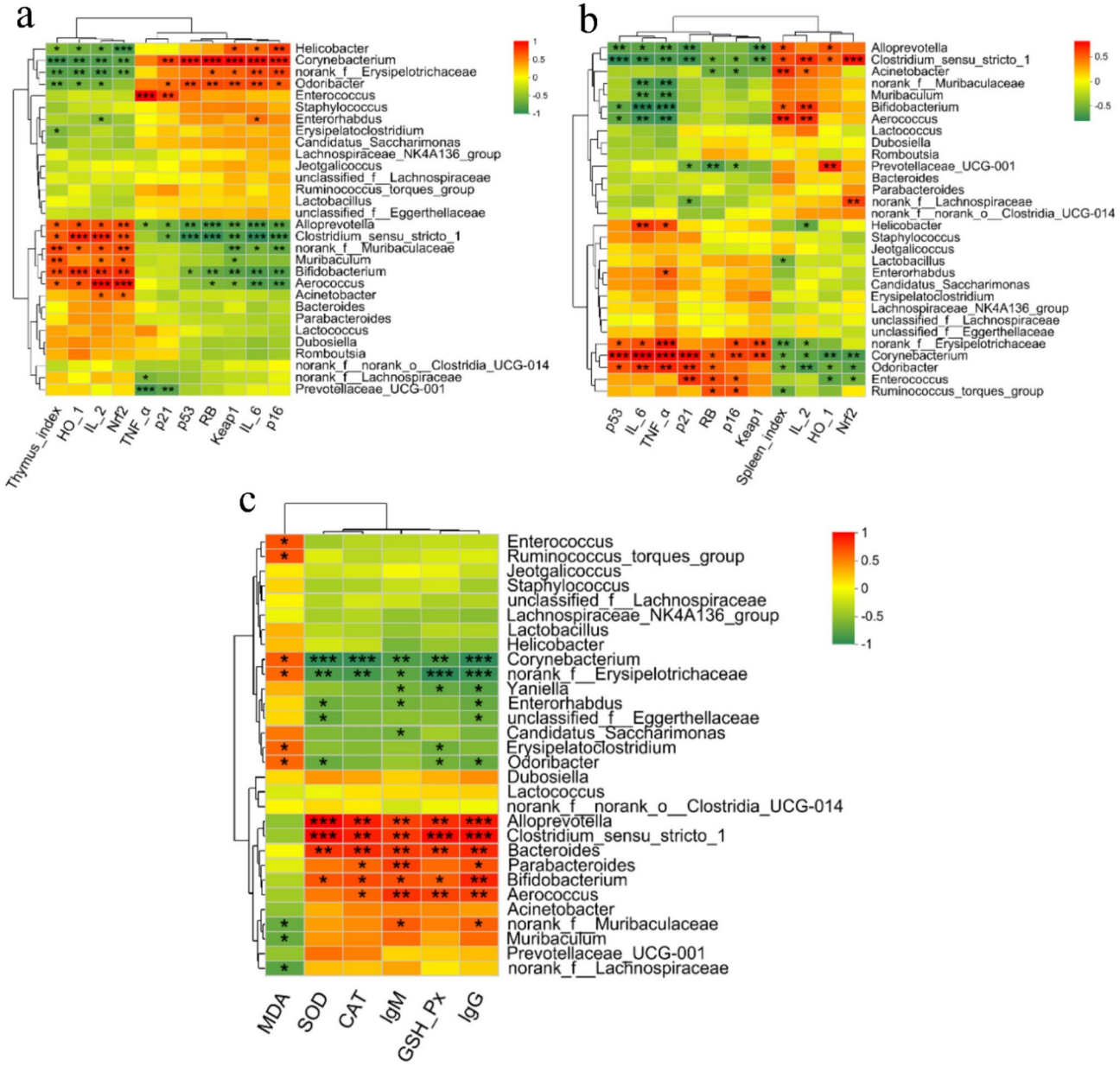

Fig. 11. Correlation analysis of gut microbiota and aging-related indicators in thymus, spleen, and serum, respectively. (**a**) Pearson analysis at the genus level in thymus tissue. (**b**) Pearson analysis at the genus level in spleen tissue. (**c**) Pearson analysis at the genus level in serum. $^{*}p < 0.05$, $^{**}p < 0.01$, and $^{***}p < 0.001$.

parameters. Collectively, these results indicate that UC-MSCs can enhance immune function and potentially delay immunosenescence.

The Nrf2/HO-1 pathway is involved in inflammation, aging, and apoptosis[35]. During aging, abnormalities in this pathway may occur. For example, the downregulation of Nrf2 protein expression reduces the production of downstream antioxidant enzymes, such as SOD, GSH-Px, and CAT, leading to diminished antioxidant capacity[36]. This makes immune organs more susceptible to oxidative damage, which accelerates the aging process. Our results showed that Nrf2 protein expression in the D-gal group was significantly downregulated, inhibiting the expression of downstream antioxidant enzymes SOD, GSH-PX, and CAT, and increasing serum oxidative stress marker MDA content. However, results from real-time quantitative PCR and immunohistochemistry show that UC-MSCs treatment significantly upregulated both the mRNA and protein levels of Keap1, Nrf2, and HO-1 compared to the D-galactose group. This finding suggests a correlation between improved antioxidant status and mesenchymal stem cell treatment, which suggests potential involvement of the Nrf2/Keap pathway.

During the aging process of immune organs, the expression of various aging-related genes undergoes significant changes[37]. Genes such as p16, p53, p21, and RB are notably upregulated in aging immune tissues[38,39]. These gene alterations impact cell cycle regulation, slowing down cell proliferation and accelerating cellular senescence, which in turn affects the functionality of immune organs[40]. Specifically, RB, p16, and p21 inhibit the

G1 phase of the cell cycle and are recognized as key markers of senescence, while p53 induces cell growth arrest, thus playing a critical role in regulating cellular aging[41]. Oxidative stress, which leads to DNA damage, further increases p53 expression. In this study, we verified the protective effect of UC-MSCs on cellular senescence by examining the gene expression levels of p53, p16, p21, and RB in the thymus and spleen. In the D-gal group, mRNA expression levels of these related genes were significantly elevated. However, treatment with UC-MSCs resulted in reduced expression levels of these genes, indicating that UC-MSCs delay cellular senescence and further improve immunosenescence by downregulating p53, p21, p16, and RB.

Numerous studies have indicated that with aging, the gut microbiota composition shifts due to the accumulation of potentially pro-inflammatory microorganisms and a reduction in beneficial organisms, resulting in decreased richness and diversity[42,43]. Our alpha diversity analysis revealed a decrease in gut microbiota diversity in the D-gal group compared to the normal group, consistent with the study of Claesson et al[44]. However, after UC-MSCs treatment, the diversity and richness of the gut microbiota increased, suggesting that UC-MSCs may improve aging conditions by improving the composition and diversity of the gut microbiota. Mesenchymal stem cells have been shown to influence the gut microbiome composition and diversity through multiple mechanisms. Firstly, MSCs can secrete various factors, such as growth factors, cytokines, chemokines, and extracellular vesicles, which can affect the growth and activity of bacteria in the gut[45]. For example, MSCs can produce interleukin-10 (IL-10), which has anti-inflammatory properties and can reduce inflammation-induced changes in the gut microbiome[46]. Secondly, MSCs directly interact with the intestinal epithelium[47]. They participate in the repair and regeneration of the intestinal barrier. A healthy and intact intestinal barrier is essential for maintaining a stable gut microbiome. When the intestinal barrier is damaged, it leads to the translocation of bacteria, which disrupts the normal composition of the gut microbiome[48]. MSCs help maintain the intestinal barrier's integrity, thus indirectly influencing the gut microbiome. Moreover, at the phylum level, the gut microbiota of mice was dominated by *Firmicutes*, *Bacteroidota*, and *Actinobacteriota*. *Actinobacteria* are considered opportunistic pathogens, and their overgrowth can negatively affect health[49,50]. Research indicates that as aging progresses, the numbers of *Firmicutes* and *Actinobacteria* increase in the elderly, while the population of beneficial bacteria, such as *Bifidobacterium*, especially those of the *Bacteroidota* phylum, decreases[51]. Our findings indicate that, in contrast to the D-gal group, treatment with UC-MSCs led to a reduction in *Firmicutes* and *Actinobacteria* while increasing *Bacteroidetes* levels. Notably, among the *Bacteroidetes*, *Alloprevotella* exhibited a negative correlation with key markers of cellular senescence such as RB, p16, p21, p53, Keap1, and MDA. Conversely, it showed a positive correlation with antioxidant defense mechanisms including Nrf2, HO-1, SOD, CAT, and GSH-PX. These associations underscore *Alloprevotella*'s potential role in mitigating oxidative stress and thereby delaying the aging process. In conclusion, UC-MSCs could alleviate D-galactose-induced gut microbiota imbalances in aging mice by increasing the diversity of gut microbiota and restoring the balance between pathogenic and beneficial bacteria.

Several limitations of this study should be acknowledged. First, while our research aimed to elucidate the role of UC-MSCs in delaying the aging process, we provided evidence of improvements in thymus and spleen pathology, activation of the Nrf2 pathway, regulation of aging-related genes, and restoration of gut microbiota balance. However, our study did not investigate all recognized biological processes contributing to aging, and we could not elucidate more specific underlying mechanisms. When evaluating immune function, we primarily focused on routine blood indicators, such as white blood cell counts and lymphocyte levels, as well as serum immunoglobulin levels IgG and IgM. Additionally, we did not observe the long-term effects of UC-MSC treatment on thymus and spleen function in aging mice. Future research should explore these aspects to gain a more comprehensive understanding of the effects of UC-MSCs on aging. Second, although 16S rDNA gene sequencing technology was employed to analyze the composition and diversity of gut microbiota, this method primarily provides information on microbial classification and relative abundance without offering insights into the functional and metabolic activity of the microbiota. Third, our experiment utilized only one mouse model. Although the D-galactose-induced aging mouse model is widely used, it may not fully replicate all physiological and pathological changes associated with natural aging. Lastly, although UC-MSCs demonstrated improvements in aging-related immune function in the mouse model, the physiological and pathological environment of the human body is considerably more complex. Multiple factors may influence the efficacy and safety of UC-MSCs, including the intricacies of the human immune system, genetic differences among individuals, and potential immune rejection reactions, all of which require further consideration.

Conclusions

Our findings suggest that UC-MSCs can down-regulate aging-marker genes such as p16, p53, p21, and RB to delay aging and mitigate D-gal-induced oxidative damage. Additionally, UC-MSCs activate the Nrf2/HO-1 pathway, enhancing the expression of antioxidant enzymes, including SOD, CAT, and GSH-PX. Furthermore, UC-MSCs improve immune dysfunction and boost overall immunity while also regulating gut microbiota composition and restoring gut homeostasis in aging mice. This study highlights the potential application of UC-MSCs in combating immune aging and provides new insights for therapeutic strategies.

Data availability

The 16S rRNA sequencing data in this study were deposited in the National Center for Biotechnology Information (NCBI) Sequence Read Archive (SRA) database under the accession number PRJNA1156233 (https://ncbi.nlm.nih.gov/bioproject/?term = PRJNA1156233). Values for all data points in graphs are reported in this manuscript.

Received: 11 August 2024; Accepted: 13 March 2025

Published online: 19 March 2025

References

1. Luo, Z. et al. Influence of demographic factors on long-term trends of premature mortality and burden due to liver cancer: Findings from a population-based study in shanghai, China, 1973–2019. *Front. Public Health* **10**, 808917 (2022).
2. Huang, J. et al. Changes of tumor infiltrating lymphocytes after core needle biopsy and the prognostic implications in early stage breast cancer: A retrospective study. *Cancer Res. Treat.* **51**, 1336–1346 (2019).
3. Aw, D. et al. Disorganization of the splenic microanatomy in ageing mice. *Immunology* **148**, 92–101 (2016).
4. Xiao, H. et al. Extracellular vesicles derived from HBMSCs improved myocardial infarction through inhibiting zinc finger antisense 1 and activating Akt/Nrf2/HO-1 pathway. *Bioengineered* **13**, 905–916 (2022).
5. Silva-Palacios, A. et al. Tert-buthylhydroquinone pre-conditioning exerts dual effects in old female rats exposed to 3-nitropropionic acid. *Redox Biol.* **12**, 610–624 (2017).
6. Qian, Y. et al. Lactobacillus plantarum CQPC11 isolated from sichuan pickled cabbages antagonizes D-galactose-induced oxidation and aging in mice. *Molecules* **23**, 3026 (2018).
7. Badal, V. D. et al. The gut microbiome, aging, and longevity: A systematic review. *Nutrients* **12**, 3759 (2020).
8. Sharma, R. et al. Dietary supplementation of milk fermented with probiotic Lactobacillus fermentum enhances systemic immune response and antioxidant capacity in aging mice. *Nutr. Res.* **34**, 968–981 (2014).
9. Roy, E., Shi, W., Duan, B. & Reid, S. P. Chikungunya virus infection impairs the function of osteogenic cells. *mSphere* **5**, e00347-e420 (2020).
10. Večerić-Haler, Ž, Kojc, N., Wechtersbach, K., Perše, M. & Erman, A. Cobalt ferrite magnetic nanoparticles for tracing mesenchymal stem cells in tissue: A preliminary study. *Int. J. Mol. Sci.* **23**, 8738 (2022).
11. Wang, Z. et al. Bone marrow mesenchymal stem cells improve thymus and spleen function of aging rats through affecting P21/PCNA and suppressing oxidative stress. *Aging (Albany NY)* **12**, 11386–11397 (2020).
12. Jung, W. S. et al. Stimulatory effect of HGF-overexpressing adipose tissue-derived mesenchymal stem cells on thymus regeneration in a rat thymus involution model. *Cell Biol. Int.* **38**, 1106–1117 (2014).
13. Kim, M. J. et al. Optimization of adipose tissue-derived mesenchymal stromal cells transplantation for bone marrow repopulation following irradiation. *World J. Stem Cells* **14**, 245–263 (2022).
14. Guenther, R. et al. The treasury of Wharton's Jelly. *Stem Cell Rev Rep* **18**, 1627–1638 (2022).
15. Zhang, Y. et al. MicroRNA-206 down-regulated human umbilical cord mesenchymal stem cells alleviate cognitive decline in D-galactose-induced aging mice. *Cell Death Discov* **8**, 304 (2022).
16. Nie, P. et al. Human umbilical cord mesenchymal stem cells reduce oxidative damage and apoptosis in diabetic nephropathy by activating Nrf2. *Stem Cell Res Ther* **12**, 450 (2021).
17. Lv, S. S. et al. Mesenchymal stem cells transplantation ameliorates glomerular injury in streptozotocin-induced diabetic nephropathy in rats via inhibiting macrophage infiltration. *Int. Immunopharmacol.* **17**, 275–282 (2013).
18. Zhang, G., Li, Y., Li, N., Shen, L. F. & Li, Z. Functional implications of aging-related lncRNAs for predicting prognosis and immune status in glioma patients. *Aging (Albany NY)* **14**, 2348–2366 (2022).
19. Connors, J. et al. Aging alters antiviral signaling pathways resulting in functional impairment in innate immunity in response to pattern recognition receptor agonists. *Geroscience* **44**, 2555–2572 (2022).
20. Michel, J. J., Griffin, P. & Vallejo, A. N. Functionally diverse NK-like T cells are effectors and predictors of successful aging. *Front Immunol.* **7**, 530 (2016).
21. Liang, Z., Dong, X., Zhang, Z., Zhang, Q. & Zhao, Y. Age-related thymic involution: Mechanisms and functional impact. *Aging Cell* **21**, e13671 (2022).
22. Yu, Z. Y. et al. Physiological clearance of Aβ by spleen and splenectomy aggravates Alzheimer-type pathogenesis. *Aging Cell* **21**, e13533 (2022).
23. de Mol, J., Kuiper, J., Tsiantoulas, D. & Foks, A. C. The dynamics of B cell aging in health and disease. *Front. Immunol.* **12**, 733566 (2021).
24. Tchkonia, T., Zhu, Y., van Deursen, J., Campisi, J. & Kirkland, J. L. Cellular senescence and the senescent secretory phenotype: Therapeutic opportunities. *J. Clin. Invest.* **123**, 966–972 (2013).
25. Niu, Y. et al. Effects of polysaccharide from Malus halliana Koehne flowers in cyclophosphamide-induced immunosuppression and oxidative stress on mice. *Oxid. Med. Cell Longev.* **2020**, 1603735 (2020).
26. He, Q. et al. Thymic development of autoreactive T cells in NOD mice is regulated in an age-dependent manner. *J. Immunol.* **191**, 5858–5866 (2013).
27. Ladomenou, F. & Gaspar, B. How to use immunoglobulin levels in investigating immune deficiencies. *Arch. Dis. Child Educ. Pract. Ed* **101**, 129–135 (2016).
28. Wang, S. et al. Effect of supplementing different levels of L-glutamine on Holstein calves during weaning. *Antioxidants Basel* **11**, 542 (2022).
29. Inci, N. et al. Transcriptomics and proteomics analyses reveal JAK signaling and inflammatory phenotypes during cellular senescence in blind mole rats: The reflections of superior biology. *Biology Basel* **11**, 1253 (2022).
30. Xiong, Y. et al. hPMSCs protects against D-galactose-induced oxidative damage of CD4(+) T cells through activating Akt-mediated Nrf2 antioxidant signaling. *Stem Cell Res. Ther.* **11**, 468 (2020).
31. van den Berk, L. C. et al. Cord blood mesenchymal stem cells propel human dendritic cells to an intermediate maturation state and boost interleukin-12 production by mature dendritic cells. *Immunology* **128**, 564–572 (2009).
32. Del Prete, A. et al. Dendritic cell subsets in cancer immunity and tumor antigen sensing. *Cell Mol. Immunol.* **20**, 432–447 (2023).
33. Fu, Y. et al. Umbilical cord mesenchymal stem cells ameliorate inflammation-related tumorigenesis via modulating macrophages. *Stem Cells Int.* **2022**, 1617229 (2022).
34. Murray, P. J. & Wynn, T. A. Protective and pathogenic functions of macrophage subsets. *Nat Rev Immunol* **11**, 723–737 (2011).
35. Yuan, M., Zhao, B., Jia, H., Zhang, C. & Zuo, X. Sinomenine ameliorates cardiac hypertrophy by activating Nrf2/ARE signaling pathway. *Bioengineered* **12**, 12778–12788 (2021).
36. Chen, M., Wen, H., Zhou, S., Yan, X. & Li, H. Patchouli alcohol inhibits D-gal induced oxidative stress and ameliorates the quality of aging cartilage via activating the Nrf2/HO-1 pathway in mice. *Oxid. Med. Cell Longev.* **2022**, 6821170 (2022).
37. Calcinotto, A. et al. Cellular senescence: Aging, cancer, and injury. *Physiol. Rev.* **99**, 1047–1078 (2019).
38. Giménez-Bastida, J. A., Ávila-Gálvez, M., Espín, J. C. & González-Sarrías, A. Conjugated physiological resveratrol metabolites induce senescence in breast cancer cells: Role of p53/p21 and p16/Rb Pathways, and ABC transporters. *Mol. Nutr. Food Res.* **63**, e1900629 (2019).
39. Salama, R., Sadaie, M., Hoare, M. & Narita, M. Cellular senescence and its effector programs. *Genes Dev.* **28**, 99–114 (2014).
40. Kumari, R. & Jat, P. Mechanisms of cellular senescence: Cell cycle arrest and senescence associated secretory phenotype. *Front. Cell Dev. Biol.* **9**, 645593 (2021).
41. Jesel, L. et al. Atrial fibrillation progression is associated with cell senescence burden as determined by p53 and p16 expression. *J. Clin. Med.* **9**, 36 (2019).
42. Du, Y. et al. Effects of anti-aging interventions on intestinal microbiota. *Gut. Microbes* **13**, 1994835 (2021).

43. Tiihonen, K., Ouwehand, A. C. & Rautonen, N. Human intestinal microbiota and healthy ageing. *Ageing Res. Rev.* **9**, 107–116 (2010).
44. Claesson, M. J. et al. Gut microbiota composition correlates with diet and health in the elderly. *Nature* **488**, 178–184 (2012).
45. Liu, A. et al. Human umbilical cord mesenchymal stem cells ameliorate colon inflammation via modulation of gut microbiota-SCFAs-immune axis. *Stem Cell Res. Ther.* **14**, 271 (2023).
46. Zou, Y. et al. Human umbilical cord mesenchymal stem cells improve disease characterization of Sjogren's syndrome in NOD mice through regulation of gut microbiota and Treg/Th17 cellular immunity. *Immun. Inflamm. Dis.* **12**, e1139 (2024).
47. Xu, J. et al. Embryonic stem cell-derived mesenchymal stem cells promote colon epithelial integrity and regeneration by elevating circulating IGF-1 in colitis mice. *Theranostics* **10**, 12204–12222 (2020).
48. Okumura, R. & Takeda, K. Maintenance of intestinal homeostasis by mucosal barriers. *Inflamm. Regen.* **38**, 5 (2018).
49. Yang, A. et al. Effects of different sources of calcium in the diet on growth performance, blood metabolic parameters, and intestinal bacterial community and function of weaned piglets. *Front. Nutr.* **9**, 885497 (2022).
50. Li, Y. et al. Lactobacillus casei improve anti-tuberculosis drugs-induced intestinal adverse reactions in rat by modulating gut microbiota and short-chain fatty acids. *Nutrients* **14**, 1668 (2022).
51. Mariat, D. et al. The Firmicutes/Bacteroidetes ratio of the human microbiota changes with age. *BMC Microbiol.* **9**, 123 (2009).

Acknowledgements

This work was supported by the National Natural Science Foundation of China (82160126), the Natural Science Foundation Project of Guizhou Provincial Science and Technology Department (grant no. Qiankehe Foundation-ZK 2024 General 182), Guizhou Medical University Doctoral Start-up Fund(XBHJ[2024]018 & [2020]018). Science and Technology Fund Project of Guizhou Province Health Commission(gzwkj2023-230), Cooperation projects of Guizhou Medical University-Guizhong Biotechnology Co., Ltd.(HY2402).

Author contributions

Jianwei Xu and Li Dong conceived and designed the study, and drafted the manuscript. Xiaofen Xie and Junhou Lu performed experiments and data analyses. Guo Ge, Zhenkui Ren, Bill D. Geng, Yongxi Dong, Yang Hu, Can Liu, and Yuanhu Mao provided critical comments and revisions on the manuscript. All authors read and approved the final manuscript.

Declarations

Competing interests

The authors declare no competing interests.

Additional information

Correspondence and requests for materials should be addressed to G.G. or Z.R.